On the Mechanism of Pore Formation in Metals

H. FREDRIKSSON AND I. SVENSSON

The formation of different types of gas pores has been investigated by directional solidification experiments. A mathematical model of pore growth has been derived and the calculated pore growth has been compared with experimental data and a good correlation was found. The nucleation process of pores has also been treated. It was shown that micropores can be homogeneously nucleated in an interdendritic area according to the pressure drop caused by the solidification shrinkage.

SEVERAL types of pores can be observed in solidified metal alloys. These pores are normally caused by gas dissolved in the metal melt. Normally the quantity of gas determines the shape of the pores. The solubility of gas in metal melts normally decreases with decreasing temperature, and if the gas content is high the solubility limits can be reached during cooling and gas precipitation starts before the solidification process. These gas bubbles float in the metal melt and normally reach the surface of the metal before the start of the solidification process.

The solubility of gas is normally lower in the solid state than in the liquid and because of this the segregation of the gas elements will give gas precipitation during the solidification process. The type of pores thus formed are often elongated as for instance the pores in the rim zone in an unkilled ingot and in welds with high hydrogen content. The formation of these pores is sometimes compared with a normal eutectic reaction and is discussed elsewhere in the literature[1-3] but the explanation of the formation process seems to be incorrect. The aim of this work was to study the formation process of this type of pore by unidirectionally controlled solidification experiments followed by a theoretical analysis.

Another type of pore which often occurs in ingots and castings at the end of the solidification process is that of micropores. They are suggested to be caused by the solidification shrinkage but it is possible that the formation of these pores is related to the gas content of the liquid. The tendency of gas precipitation will increase because the supersaturation increases when the pressure decreases in the interdendritic area at the end of the solidification process. The formation of this type of pore will also be discussed in this paper.

EXPERIMENTS

Stainless steel containing 25 wt pct Ni 20 pct Cr and 3 pct Mo was used in this work. DTA (differental thermal analysis) experiments showed that the alloy solidified directly to austenite. The liquidus temperature was determined to 1430°C and the alloy had a freezing range of 55°C.

H. FREDRIKSSON is Professor and I. SVENSSON is with the Department of Casting of Metals, The Royal Institute of Technology, Stockholm, Sweden.

Manuscript submitted January 29, 1976.

The equipment for the unidirectional solidification experiments is shown in Fig. 1. The alloy was melted in a crucible at the lower end of the furnace. A water-cooled probe was placed at the upper part of the furnace. Between the crucible and the probe a sucepter of Mo was placed. A sharp temperature gradient existed between the probe and the sucepter. The alloy was sucked up into an alumina tube ($4 \cdot 10^{-3}$ m external diameter and $3 \cdot 10^{-3}$ m internal diam). The probe caused the upper part of the alloy in the tube to solidify. The plug thus formed prevented the melt from dropping out of the tube during the experiment. Just after the sucking, the experiment was started by pulling the tube out of the furnace through the probe at a constant rate.

The alloy was studied at three different solidification rates, 0.018, 0.009 and 0.0035 m/s, and with three different hydrogen contents, 14, 16 and 18 ppm. The hydrogen content in the samples was controlled by the furnace atmosphere – a mixture of Ar and H_2

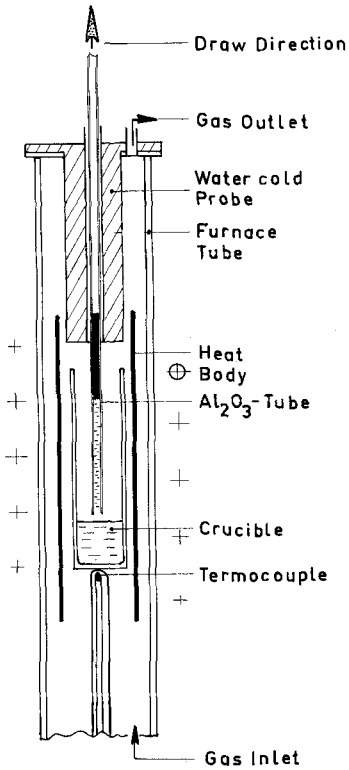

Fig. 1—Cross section of the experimental equipment.

was used—and by changing the partial pressure of H_2 different hydrogen contents were obtained. In order to get the correct hydrogen content the alloy was melted and held for 1800 s before sucking the alloy into the tube.

In order to determine the solubility of hydrogen in the alloy, phase-equilibrium-experiments were carried out. Four experiments were made, two over and two under the liquidus temperature. The technique used for the phase equilibrium experiments are described in the next paragraph.

HYDROGEN EQUILIBRIUM MEASUREMENTS

The equilibrium experiments below the solidus temperature were made at 1360 and 1390°C. In this case the alloy was melted, sucked up into a thin walled Al_2O_3 tube, and then quenched in brine. The tube was removed and the samples were placed in a tube-furnace at the above mentioned temperature. In order to homogenize the sample it was held for 2 h at the temperature and the furnace atmosphere was pure hydrogen. The samples were then quenched in brine and immediately transferred to a cold-mixture of solid CO_2 and alcohol.

The equilibrium experiments above the liquidus temperature were made at 1440 and 1490°C. The samples were melted in an Al_2O_3 crucible and heat-treated for 1800 s in a gas-atmosphere of 85 pct Ar and 15 pct H_2. This lower hydrogen pressure was used to avoid pore-formation during solidification when the sample was quenched in brine. After quenching the samples were transferred to the cold-mixture. The hydrogen content was analyzed in degassing instrument of type LECO RH-JE. The samples were heated to 2600°C and the emitted gas was analyzed by gas-chromatrography.

The results of the hydrogen content measurements are shown in Table I. The table also shows the hydrogen content converted to 1 atm. That data is plotted in Fig. 2 and by the extrapolation of the data the distribution constant between γ/L was calculated to $k^{\gamma/L} = 0.47$. In the diagram (Fig. 2) the solubility of hydrogen in pure iron is added.[4] It shows clearly that the solubility is somewhat higher in the investigated stainless steel examined both in the solid- and in the liquid state.

THE CONTROLLED SOLIDIFICATION EXPERIMENTS

A series of introduction experiments were carried out at different hydrogen contents and at different speeds. The experiment showed that it was impossible to get elongated pores of the type we wanted to

Table I. The Solubility of Hydrogen in the Steel

Temperature	ppm H $p_{H_2} = 0.15$ atm	ppm H $p_{H_2} = 1$ atm
1360	–	12.12
1390	–	12.13
1440	9.69	25.74
1490	10.30	27.36

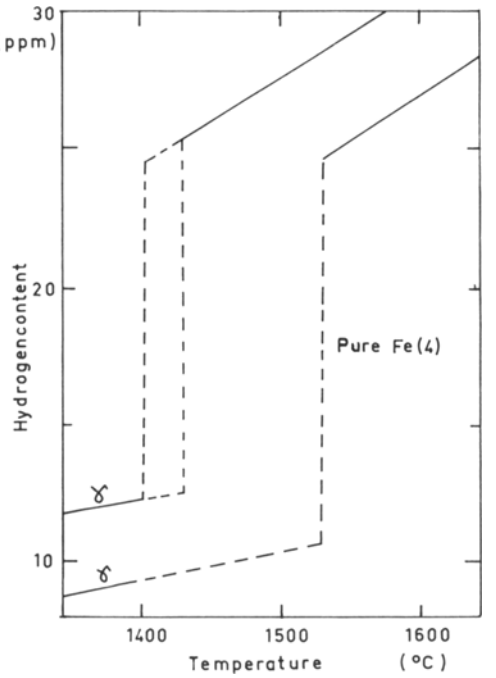

Fig. 2—The solubility of hydrogen in an austenitic stainless steel at 1 atm and the solubility of hydrogen in pure iron according to Ref. 4.

study. However, a large number of micropores were observed (Figs. 3 and 4). It was observed that the numbers of this type of pore increased with increasing hydrogen content and with increasing solidification rate. The conclusion was that the gas content in the melt favors the formation of this type of pore.

In order to induce nucleation of the type of macropores we wanted to study small amounts of Al_2O_3 powder which was added to the melt before the start of the experiment. This addition induced the formation of macropores and at the starting point of every large observed pore one or more Al_2O_3 grains could be observed. It is easy to suggest that the pores are nucleated by Al_2O_3 inclusions.

In the experiments with 16 and 18 ppm hydrogen large elongated pores of the type shown in Figs. 5 and 6 were formed. The figures show that the pores increase in diameter from the starting point. A com-

Fig. 3—Micropores in a sample with 16 ppm H and solidified with a rate of 54 cm/min, magnification 70 times.

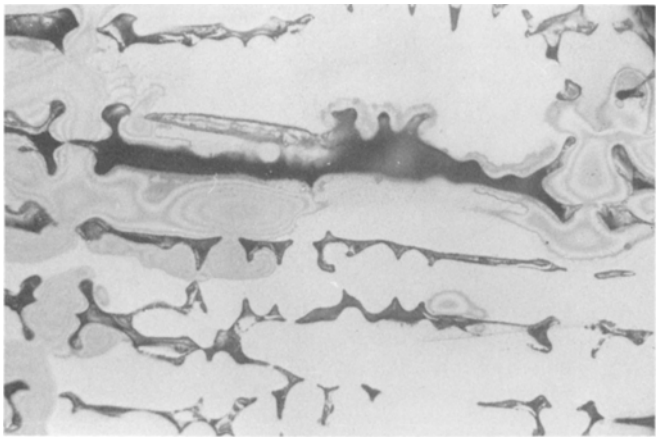

Fig. 4—Higher magnification of Fig. 3, magnification 350 times.

parison between Figs. 5 and 6 shows that the diameter increases with a decreasing solidification rate and an increasing hydrogen content. Further, it is of interest to note from the figures that the walls of the pores are corrugated. At the lowest speed and at 18 ppm hydrogen the growth of pore diameter is so rapid that the pores block the growth of the solid phase, Fig. 6(*a*).

In the samples with 14 ppm hydrogen, elongated macropores could not be observed even with the addition of Al_2O_3 powder. However, in the presence of some of the small dispersive Al_2O_3 particles, pores of the type shown in Fig. 7 were observed. With this hydrogen content the pores were not compatible with the growing solidification front. The pores were soon surrounded and isolated by the solid material.

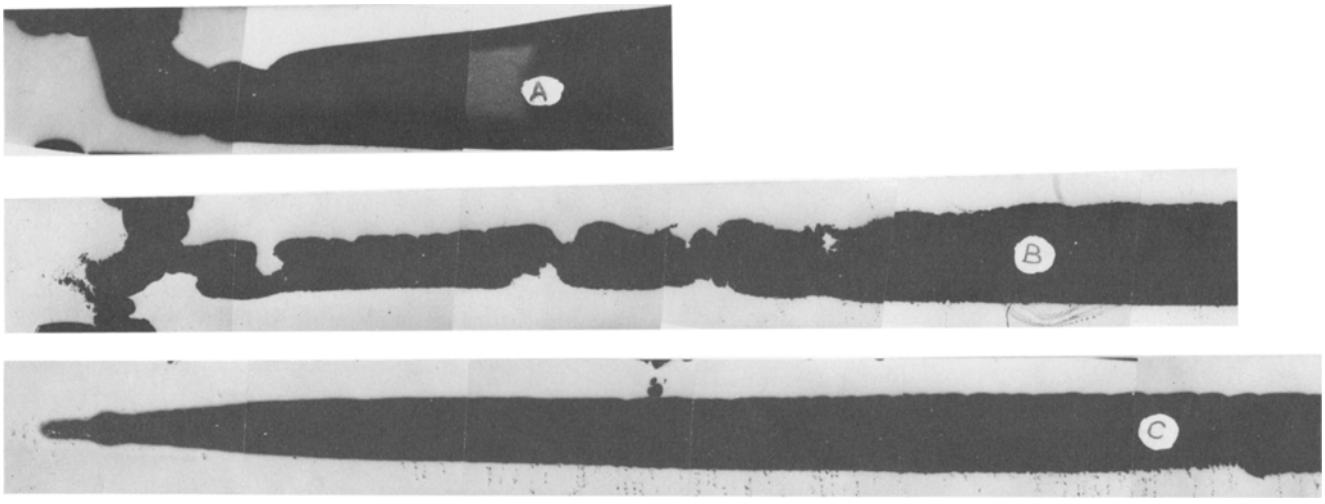

Fig. 5—Unidirectionally solidified samples with elongated macropores in an alloy with 16 ppm H. Solidification direction from the left to the right. Solidification rate (*a*) 0.0035 m/s, (*b*) 0.009 m/s, (*c*) 0.018 m/s, magnification 6.6 times.

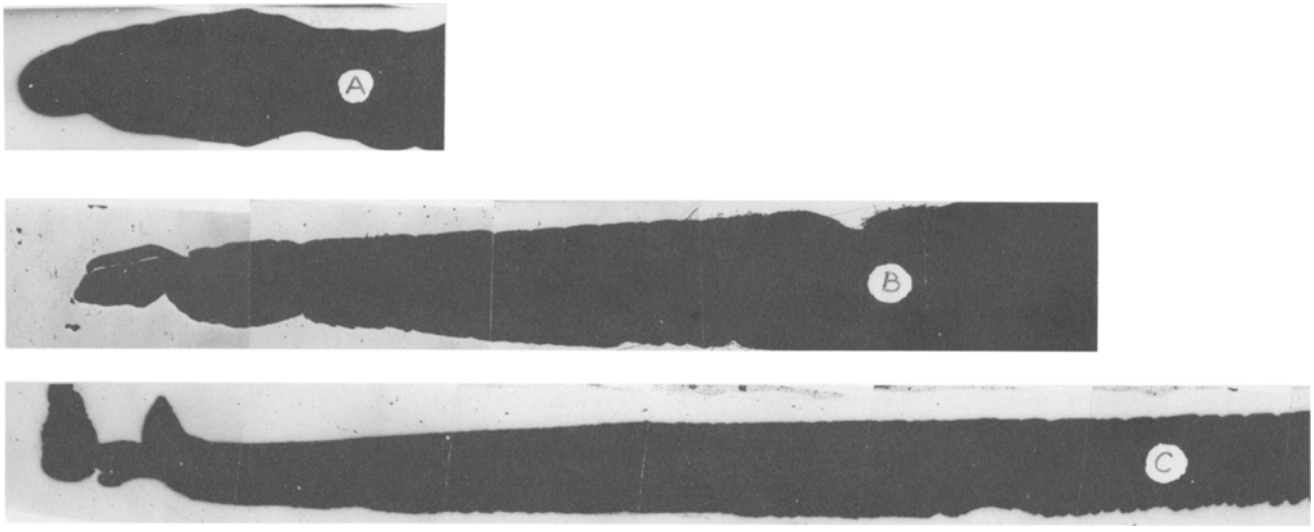

Fig. 6—Unidirectionally solidified samples with elongated macropores in an alloy with 18 ppm H. Solidification direction from the left to the right. Solidification rate (*a*) 0.0035 m/s, (*b*) 0.009 m/s, (*c*) 0.018 m/s, magnification 6.6 times.

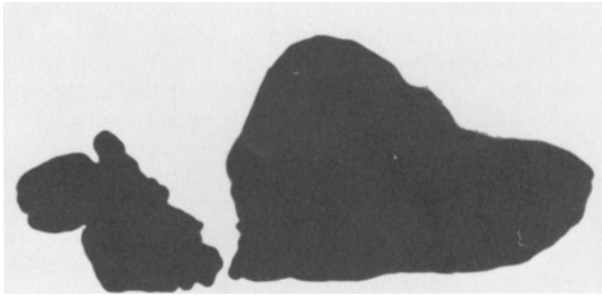

Fig. 7—Partly elongated macropore in a unidirectionally solidified sample with 14 ppm H. The pore has been overgrown by the solidification front. Solidification direction from the left to the right. Solidification rate 0.0035 m/s.

DISCUSSION

Segregation of Hydrogen

The diffusion constant of hydrogen in austenite at 1400°C is roughly 10^{-8} m^2/s and in the melt about 10 times larger.[5] In calculations of segregation in iron-base-alloys it has been shown[6,7] that the level-rule is a good approximation at diffusion-constants larger than 10^{-10} m^2/s. We can then use the following formula for calculating the hydrogen content in the melt as a function of fraction solid material

$$C_H^L = \frac{C_H^o}{[1 - f(1 - k)]} \qquad [1]$$

where

C_H^o = the original hydrogen content,
f = the fraction solid material,
k = the partition coefficient between austenite and liquid.

Fig. 8 shows the hydrogen content in the melt as a function of fraction solid material for 14, 16 and 18 ppm hydrogen. In the figure the solubility limits for hydrogen in the liquid and in the austenite at one atmosphere pressure have been added, according to the measurements shown in a previous chapter. The figure shows that the solubility limits at the three hydrogen levels in the alloy are exceeded at a fraction of solid material of 0.85, 0.70 and 0.55 respectively. It is possible for a gas pore to be fromed at these fractions of solid material. However, the experiments showed that the nucleation of the pores was difficult. In the next chapter the question about the possibility for homogeneous nucleation of a pore will be discussed.

The Nucleation Process

The theory of homogeneous nucleation has been penetrated by several authors in the literature.[8-10] All papers have treated the case of pore formation when pure substances reach their boiling point. In this case the theory leads to a very high supersaturation for homogeneous nucleation. This theory is also adaptable to the formation of hydrogen gaspores in steel. However, the calculations of the driving force must be modified. Hirth *et al*[10] have recently made a very good summary of the nucleation process for gas pores and we will adapt their treatings in this paper. The activation energy for nucleation can be described by the formula

$$\Delta F^* = \frac{16\pi \cdot \sigma^3}{3(\Delta F_v)^2} \qquad [2]$$

and

$$\Delta F_v = \frac{RT}{V_m^L} \cdot \ln \frac{P_r}{P_e} \qquad [3]$$

where

F_v = the Helmholz free energy,
P_r = the gas pressure in the bubble,
P_e = equilibrium pressure of the gas in the steel-melt,
σ = the surface tension between gas/metal melt,
V_M^L = partial molar volume of hydrogen in the steel melt,
T = temperature, K.

For calculation of the driving forces, ΔF_v, we have to apply the formula of Turnbull *et al*[11-12] for the activation energy ΔF^* = 60 kT. Putting this expression into Eqs. [2] and [3] the ratio between P_r and P_e will be 5.13. Assuming that Sieverts law is valid for hydrogen solution in the metal liquid the hydrogen content for homogeneous nucleation will be $\sqrt{5.13}$ times the solubility of hydrogen. The critical composition for homogeneous nucleation at 10^5 N/m^2 calculated according to this formula is shown in Fig. 8. We find that this limit will not be exceeded at any hydrogen content. The limit may be exceeded by lowering the pressure. This happens during the solidification process in an interdendritic area because

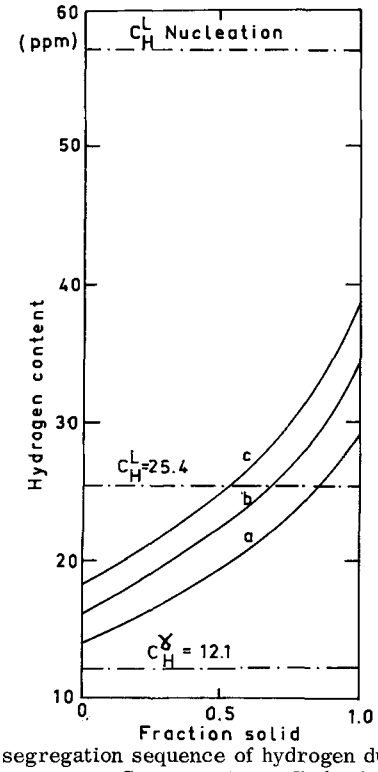

Fig. 8—The segregation sequence of hydrogen during the solidification process. Curve a 14 ppm H, b 16 ppm H, c 18 ppm H. The solubility of hydrogen at a pressure of 10^5 N/m^2 is also shown. The upper curve shows the concentration of hydrogen for nucleation of a gas pore at a pressure of 10^5 N/m^2.

of the solidification shrinkage. We will discuss this later on.

Normal *vs* Degenerated Eutectic Reaction

The experiments show that if a gas pore is nucleated, growth can occur in three principal ways.

I) The solidification front grows faster than the gas pore, resulting in small pores surrounded by solid metal. Fig. 7 gives an example of this type of pore.

II) The pore and the solidification front grow at the same speed. Fig. 5(*b*) and (*c*) shows examples of this type of pore.

III) The growth of the gas pore is so quick that it overgrows the solidification front and blocks the solidification growth. Fig. 6(*a*) gives an example of this type of pore.

During the normal dendritic growth the gas components segregate to the interdendritic areas and at a certain distance behind the front the solubility is exceeded. If a gas pore has been nucleated the hydrogen diffuses from these supersaturated areas to the nucleated pore. The growth rate of the gas pore is now determined by the amount of hydrogen reaching the pore per time. At the same time as the gas pore grows, the solidification front grows. The relation between the two growth rates determines the diameter of the gas pore and it also determines if the diameter will increase, decrease or remain constant. The solidification rate and the amount of hydrogen governs the pore formation process.

Theoretical Treatment of Pore-Growth

A numerical method of calculating pore radius as a function of the pore length, solidification rate and hydrogen content is described below. The method is based on a mass balance between the amount of hydrogen which reaches the pore wall by diffusion and the amount of hydrogen which is needed for the volume-change at the solidification front.

Fig. 9 shows a schematic diagram of the system and the figure defines the geometrical relations which are used in the calculations. In our calculations we have assumed that the diffusion of hydrogen only occurs horizontally in each volume element, Δy. The mass flow is estimated from Einstein's relation of random walks in one-dimension. We have assumed that the concentration distribution in each volume element is the one shown in Fig. 9(*b*). During a short time, Δt, every volume-element gives the following number of hydrogen moles to the pore

$$\frac{(x_H^L - x_H^o)}{V_m^H} \cdot \Delta y(R_0^2 - R_\theta^2).$$

The total amount of hydrogen which during the time period, Δt, is emitted to the pore is equal to the sum of the amount of hydrogen from all the volume elements.

$$\Delta n = \sum_0^y \frac{(x_H^L - x_H^o)}{V_m^H} \pi \cdot \Delta y(R_0^2 - R_\theta^2) \qquad [4]$$

where: Δn = the total amount of hydrogen moles which reach the pore wall,

$$R_0 = \sqrt{2D \cdot t(I)} + r(I), \qquad [5]$$

$$R_\theta = \sqrt{2D(t(I) - \Delta t)} + r(I), \qquad [6]$$

$r(I)$ is the radius of the pore in the observed volume element,

$t(I)$ is the time since the solidification front passed the observed volume element.

The connection $v = \Delta y/\Delta t$ where v = solidification rate, gives the relation between length-step and time-step. In conditions of constant pressure in the pore there is equality between the number of moles Δn, which are reaching the pore wall and the number of moles in the newly formed pore volume $\pi r^2 \Delta y$ at the solidification front

$$\Delta n = \frac{P_{H_2} \cdot r^2 \cdot \pi \cdot \Delta y}{R \cdot T} \qquad [7]$$

where

P_{H_2} = the gas pressure in the pore
r = the radius of the pore at the solidification front.

The combination of Eqs. [4] and [7] gives the pore radius at the solidification front as a function of the distances from the starting point

$$r^2 = \frac{R \cdot T}{P_{H_2} \pi \Delta y} \sum_0^y \frac{(x_H^L - x_H^o)}{V_m^H} \pi \Delta y [R_0^2 - R_\theta^2]. \qquad [8]$$

The Result of the Calculation

Eq. [8] was solved with the help of a computer. The same solidification rates and the same hydrogen contents used in the experiments were used in the calculations. In the calculations, the size of the sample

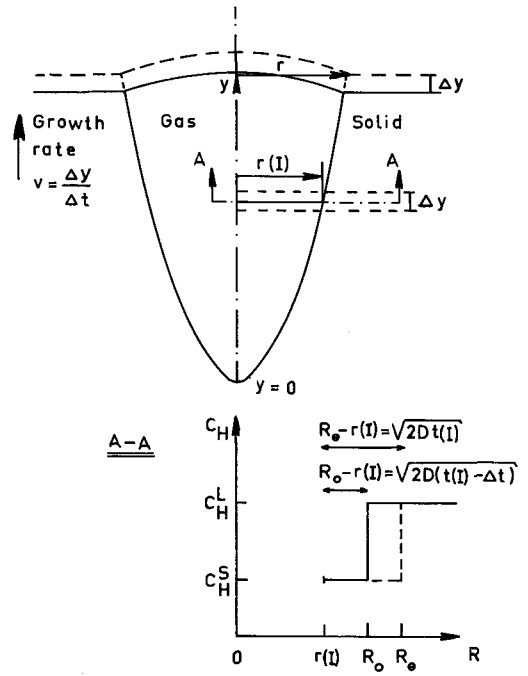

Fig. 9—Schematic representation of a macropore with the definition of the quantities in the mathematical model. The lower part shows the assumed concentration profile of H along *A-A* in the upper part of the figure.

was considered in the following way. R was allowed to grow according to Einstein's equation. Until R reached the surface of the specimen and was subsequently kept constant. The results of the calculations are given in Fig. 10(a) through (c).

In Fig. 11 a comparison is made between the growth rate of the pore in Fig. 6(c) and the calculated pore growth. It is observed from the figure that the agreement is very good at the beginning of the pore growth. However, a deviation can be observed with increasing pore-length. Here the calculated pore radius is larger than that obtained in the experiment. This is probably doe to the influence of the specimen-surface being greater than the model could tolerate, and in the case of larger pore-radii, some hydrogen escaping from the surface.

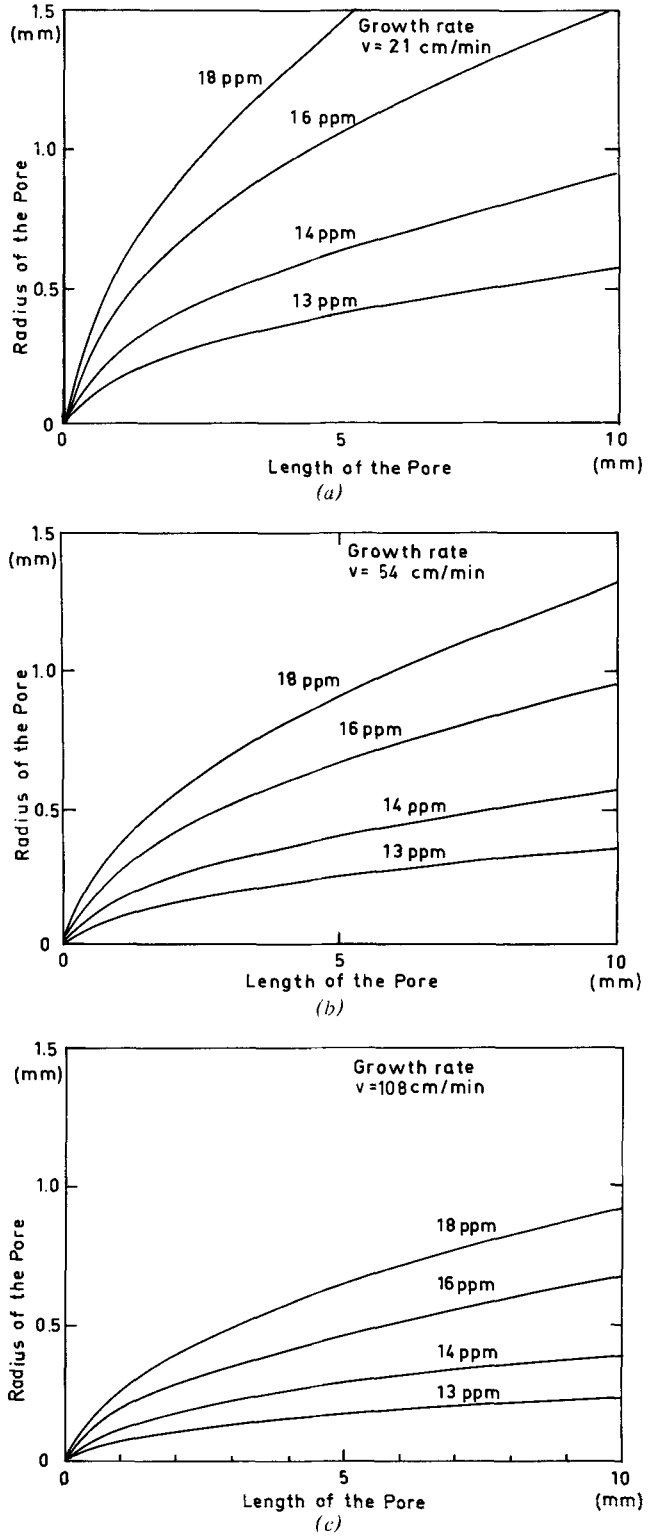

Fig. 10—Calculated pore size as a function of the distance from the starting point for different hydrogen contents. Solidification rates (a) 0.0035 m/s, (b) 0.009 m/s, (c) 0.018 m/s.

At slow solidification rates and high supersaturation the calculations showed that the pore radius growth was so rapid that the pore reached the wall and blocked the growth of the solid phase. The same thing was observed experimentally and was illustrated in Fig. 7(a).

The Formation Process of Micropores

It has earlier been pointed out, that the pressure decreases during the solidification process in an interdendritic area as a consequence of the solidification shrinkage. We will now try to investigate the possibility of obtaining such a low pressure in an interdendritic area that homogeneous nucleation occurs. Flemings *et al*[13,14] have made calculations of the pressure drop in an interdendritic area according to the solidification shrinkage. We have adopted their methods. However, the equations have been modified so that the pressure can be calculated as a function of the remaining fraction liquid. (See Appendix). The results of the calculations for the different speeds are given in Fig. 12.

As the pressure decreases in an interdendritic area, the solubility limit of hydrogen also decreases in this area. The decrease of the solubility limits as a function of fraction solid can be calculated from Sieverts law and the result of such a calculation is shown in Fig. 13 for the pressure drops shown in Fig. 12. In Fig. 13 a line representing the segregation of hydrogen in an alloy with 14 ppm H is also shown.

In the same way the solubility limit for homogeneous nucleation is influenced and this is also shown in Fig. 13. From the figure we can see that homogeneous nucleation of a gas pore is possible in an interdendritic area if we take into account the pressure

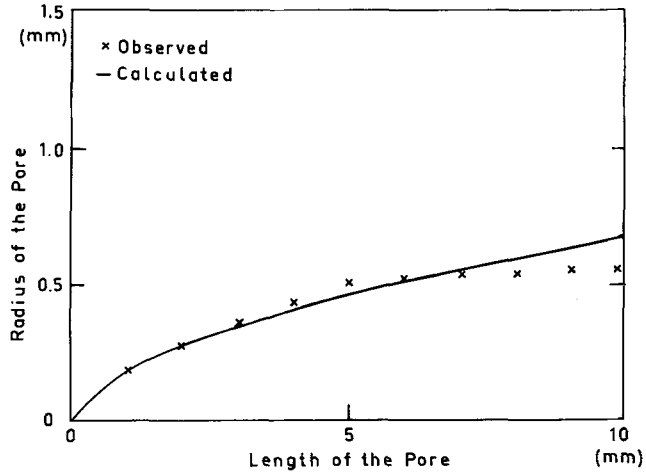

Fig. 11—A comparison between calculated and experimental pore growth, solidification rate 108 cm/min, hydrogen content 16 ppm.

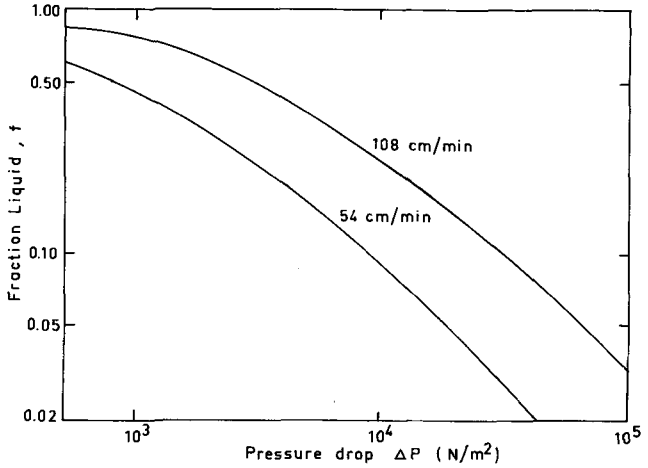

Fig. 12—The pressure drop according to the solidification shrinkage as a function of fraction of remaining liquid. Solidification rate 0.0035 m/s and 0.009 m/s.

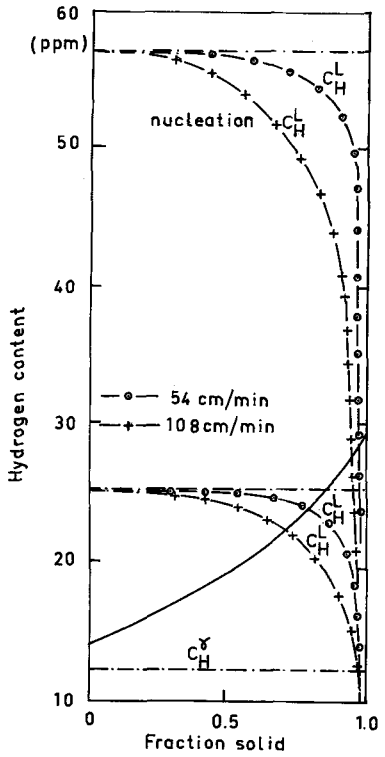

Fig. 13—The segregation sequence of hydrogen according to Fig. 8. The solubility of hydrogen in the liquid and the concentration of hydrogen for nucleation of a gas pore has been adjusted for the pressure drop according to the solidification shrinkage.

drop according to the solidification shrinkage. The possibilities increase with increasing solidification rate. It is furthermore interesting to note that the possibility for homogeneous nucleation increases with increasing solidification-range (Appendix Eq. [4]) and with increasing hydrogen content. When the pore is nucleated the pressure in the interdendritic area increases due to the large volume of the gas phase and the growth of the pore will slow down. This process will probably lead to the formation of the type of micropores shown in Figs. 3 and 4.

CONCLUSION

The formation process of different types of gas pores has been studied by the directional solidification technique. Specimens of an austenitic stainless steel containing different amounts of hydrogen gas were solidified at various rates.

The formation sequence of elongated pores of the type appearing in the riming zone in unkilled ingots was studied as a function of gas content and solidification speed.

A mathematical model for gas pore growth has been derived and computer calculations have been made. The results of the experiments have been compared with calculated data and good conformity has been obtained. The nucleation sequence for the different types of pores has been discussed in the paper.

The influence of gas contents and the influence of the solidification rates on the formation process of micropores has been studied. It has been shown that, these pores have been formed by homogeneous nucleation of gas pores in an interdendritic area. The possibilities for homogeneous nucleation of gas pores are caused by the pressure drop formed according to the solidification shrinkage.

APPENDIX

According to Flemings *et al*[13,14] the pressure drop in the interdendritic region can be written

$$\frac{dP}{dl} = \frac{8\mu v}{r^2} \qquad [A1]$$

where

r = the size of an interdendritic channel,
μ = the liquid viscosity,
v = the liquid velocity.

v is related to the solidification rate, V, by the expression

$$v = \frac{\beta}{1-\beta} \cdot V \qquad [A2]$$

where

β = the solidification shrinkage.

The size of the interdendritic channel r, is related to the dendrite space and the fraction remining liquid by the expression

$$r = \frac{L-l}{L} \frac{\lambda}{2} \qquad [A3]$$

where

λ = the primary dendrite space,
L = the length of the mushy zone,
$L - l$ = the distance from the solidification front.

Combining Eqs. [1], [2] and [3] and integrating gives the pressure drop in the mushy zone

$$\Delta P = \frac{\beta}{1-\beta} \frac{V \cdot 16 \cdot L}{\lambda^2} \frac{(L-l)}{l} . \qquad [A4]$$

This equation has been solved with the following parameters

$\beta = 0.05$,
$V = 0.018$ and 0.009 m/s,
$\lambda = 0.1 \cdot 10^{-6}$ m and $0.14 \cdot 10^{-6}$ m at respectively rate,
$\mu = 5.4 \cdot 1'^{-3}$ Ns/m^2,
$L = 5 \cdot 10^{-3}$ m.

REFERENCES

1. T. Wada: National *Res. Inst. Metals Trans.*, 1966, vol. 8, pp. 136-43.
2. G. M. Grigorenko: *Avd. Svarka*, 1970, vol. 10, pp. 13-17.
3. D. Burns, J. Beech: *"Growth of Blowholes During the Solidification of Iron-Base Alloys," Chemical Metallurgy of Iron and Steel,* Iron Steel Inst., 1971.
4. J. D. Fast: *Interaction of Metals and Gases,* Philips, Eindhoven, 1965.
5. H. Baster and K. W. Lange: *Arch. Eisenhüettenw.*, 1972, vol. 43, p. 208.
6. Y. Chuang, W. Wepner, and K. Schwerdtfeger: *Arch. Eisenhuettenw.*, 1973, vol. 44, pp. 243-50.
7. H. Fredriksson: *Scand. J. Met.*, 1976, vol. 4, pp. 27-32.
8. W. Döring: *Z. Phys. Chem.*, 1937, vol. 36B, pp. 371-86.
9. J. P. Hirth and G. M. Pound: *Condensation and Evaporation,* Pergamon Press, Oxford, 1963.
10. J. P. Hirth, G. M. Pound and G. R. Pierre: *Met. Trans.*, 1970, vol. 1, pp. 939-45.
11. J. C. Fisher, J. H. Hollman, and D. Turnbull: *J. Appl. Phys.*, 1948, vol. 19, pp. 775-84.
12. D. Turnbull and J. C. Fischer: *J. Chem. Phys.*, 1949, vol. 17, pp. 71-73.
13. T. S. Piwonka and M. C. Flemings: *Trans. TMS-AIME,* 1966, vol. 236, pp. 1157-65.
14. R. L. Coble and M. C. Flemings: *Met. Trans.*, 1971, vol. 2, pp. 409-14.